Inorg. Chem. **2009**, *48*, 1928−1937

Matrix Effects on the Triplet State of the OLED Emitter Ir(4,6-dFppy)$_2$(pic) (FIrpic): Investigations by High-Resolution Optical Spectroscopy

Andreas F. Rausch,[†] Mark E. Thompson,[‡] and Hartmut Yersin*[,†]

Universität Regensburg, Institut für Physikalische and Theoretische Chemie, 93053 Regensburg, Germany, and University of Southern California, Department of Chemistry, Los Angeles, California 90089

Received July 4, 2008

The sky-blue emitting compound Ir(4,6-dFppy)$_2$(pic) (iridium(III)bis[2-(4′,6′-difluorophenyl)pyridinato-N,C$^{2'}$]-picolinate), commonly referred to as FIrpic and representing a well-known emitter material for organic light emitting diodes (OLEDs), has been investigated in detail by optical spectroscopy. Studies at temperatures from $T = 1.5$ K to $T =$ 300 K were carried out in CH_2Cl_2 and tetrahydrofuran (THF). In CH_2Cl_2, two discrete sites were observed at cryogenic temperatures and studied by site-selective, high-resolution spectroscopy. The investigations reveal that the molecules located at the two sites exhibit distinctly different photophysical properties. For example, the three substates I, II, and III of the emitting triplet state T_1 of the low-energy site A show a distinctly larger zero-field splitting (ZFS) and exhibit shorter individual decay times than observed for the high-energy site B. The vibrational satellite structures in the emission spectra of the substates I(A) and I(B) exhibit clear differences in the ranges of metal−ligand (M−L) vibrations. For the compound studied in a polycrystalline THF host, giving only strongly inhomogeneously broadened spectra, the ZFS parameters and substate decay times vary in a similar range as observed for the two discrete sites in the CH_2Cl_2 matrix. Thus, the amount of ZFS, the emission decay times, and also the intensities of the M−L vibrational satellites are affected by the matrix cage, that is, the host environment of the emitting complex. These properties are discussed with respect to variations of spin−orbit coupling routes. In particular, changes of d-orbital admixtures, that is, differences of the metal-to-ligand charge transfer (MLCT) character in the emitting triplet, play an important role. The matrix effects are expected to be also of importance for FIrpic and other Ir(III) compounds when applied as emitters in amorphous OLED matrixes.

1. Introduction

In recent years, phosphorescent organo-transition metal compounds have come into the focus of research, as they represent efficient emitters for organic light emitting diodes (OLEDs).[1−21] Because of strong spin−orbit coupling (SOC) between the lowest triplet state and higher lying singlet states induced by the heavy metal center, these phosphorescent materials allow both singlet and triplet excitons to be utilized for generating electroluminescence (triplet harvesting).[3−5] Among these triplet emitters, a well-known compound is

* To whom correspondence should be addressed. E-mail: hartmut.yersin@chemie.uni-regensburg.de.
† Universität Regensburg.
‡ University of Southern California.

(1) *Highly Efficient OLEDs with Phosphorescent Materials*; Yersin, H., Ed.; Wiley-VCH: Weinheim, 2008.
(2) Hirani, B.; Li, J.; Djurovich, P. I.; Yousufuddin, M.; Oxgaard, J.; Persson, P.; Wilson, S. R.; Bau, R.; Goddard, W. A., III.; Thompson, M. E. *Inorg. Chem.* **2007**, *46*, 3865–3875.
(3) Adachi, C.; Baldo, M. A.; Thompson, M. E.; Forrest, S. R. *J. Appl. Phys.* **2001**, *90*, 5048–5051.
(4) Ikai, M.; Tokito, S.; Sakamoto, Y.; Suzuki, T.; Taga, Y. *Appl. Phys. Lett.* **2001**, *79*, 156–158.
(5) Yersin, H. *Top. Curr. Chem.* **2004**, *241*, 1–26.
(6) Adachi, C.; Kwong, R. C.; Djurovich, P. I.; Adamovich, V.; Baldo, M. A.; Thompson, M. E.; Forrest, S. R. *Appl. Phys. Lett.* **2001**, *79*, 2082–2084.
(7) Kawamura, Y.; Goushi, K.; Brooks, J.; Brown, J. J.; Sasabe, H.; Adachi, C. *Appl. Phys. Lett.* **2005**, *86*, 071104. (1−3).
(8) Holmes, R. J.; Forrest, S. R.; Tung, Y.-J.; Kwong, R. C.; Brown, J. J.; Garon, S.; Thompson, M. E. *Appl. Phys. Lett.* **2003**, *82*, 2422–2424.
(9) Tokito, S.; Iijima, T.; Suzuri, Y.; Kita, H.; Tsuzuki, T.; Sato, F. *Appl. Phys. Lett.* **2003**, *83*, 569–571.
(10) Yang, X. H.; Jaiser, F.; Klinger, S.; Neher, D. *Appl. Phys. Lett.* **2006**, *88*, 021107. (1−3).
(11) Vecchi, P. A.; Padmaperuma, A. B.; Qiao, H.; Sapochak, L. S.; Burrows, P. E. *Org. Lett.* **2006**, *8*, 4211–4214.

10.1021/ic801250g CCC: $40.75
Published on Web 01/27/2009

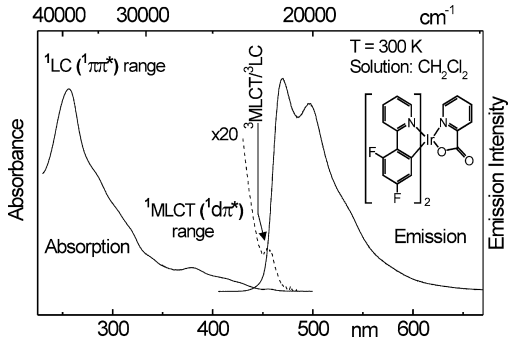

Figure 1. Absorption and emission of Ir(4,6-dFppy)$_2$(pic) (FIrpic) in CH_2Cl_2 ($c \approx 5 \times 10^{-5}$ mol/L, $\lambda_{exc} = 300$ nm) at $T = 300$ K. The dashed line, showing the absorption in the region of the lowest excited state, is scaled by a factor of 20.

Ir(4,6-dFppy)$_2$(pic) (or FIrpic) (see inset of Figure 1), which exhibits high emission quantum yields of about 60% in solution[6] and of almost 100% in a solid film.[7] It has been shown that this compound represents an excellent dopant for efficient sky-blue emitting OLEDs.[6,8−16] By using a novel bipolar host material with a high triplet energy, an OLED device with 24% external quantum efficiency and a power efficiency of 46 lm/W at 100 cd/m^2 has been realized.[17] Tuning of the emission color of FIrpic to a saturated blue has been obtained by adjusting the electroluminescence spectrum with a microcavity OLED.[18] Also white light emitting OLEDs, using FIrpic together with longer wavelength emitters in multilayer structures, have been produced.[19,20] Beside its attractiveness as emitter, FIrpic has also been utilized as hole blocking and electron transport material[21] and as phosphorescence sensitizer for an orange-emitting Cu(I) compound.[22] Motivated by these interesting applications, the electrochemical properties of FIrpic,[23,24] energy transfer and quenching behavior in different host materials,[7,25−28] exciton diffusion,[19] and X-ray absorption and resonant photoemission[29] have also been studied.

Despite the attractiveness of FIrpic, only few reports deal with the nature of the lowest excited electronic state.[30,31] Since important photophysical parameters, such as emission decay time and phosphorescence quantum yield, are determined by the individual triplet substates even at ambient temperature, it is of interest to study these substates and their properties in detail. Therefore, we investigated this compound down to cryogenic temperatures on the basis of high-resolution site-selective emission and excitation spectroscopy in different host materials. Interestingly, the results reveal that the electronic and vibronic properties vary significantly for different environments of the FIrpic dopants.

2. Experimental Section

Synthesis. FIrpic was synthesized according to the procedure described in ref 32.

Spectroscopy. Spectroscopic measurements were carried out with FIrpic dissolved in CH_2Cl_2 and tetrahydrofuran (THF) with a concentration of about 5×10^{-5} mol/L and of about 1×10^{-5} mol/L, respectively. Absorption spectra were recorded with a Varian Cary 300 double beam spectrometer. Emission spectra at 300 K were measured with a steady-state fluorescence spectrometer (Jobin Yvon Fluorolog 3). Experiments at lower temperatures were carried out in a He cryostat (Cryovac Konti Cryostat IT) in which the He gas flow, He pressure, and heating were controlled. A pulsed Nd:YAG laser (IB Laser Inc., DiNY pQ 02) with a pulse width of about 7 ns was applied for UV excitation and as excitation source for lifetime measurements, using the third harmonic at 355 nm (28170 cm^{-1}). For selective excitation, a pulsed dye laser (Lambdaphysik Scanmate 2C) with Coumarin 120 was operated. The spectra were recorded with an intensified CCD camera (Princeton PIMAX) or a cooled photomultiplier (RCA C7164R) attached to a triple spectrograph (S&I Trivista TR 555). Decay times were registered using a FAST Comtec multichannel scaler PCI card with a time resolution of 250 ps.

3. Results and Discussion

3.1. Spectroscopic Introduction. To introduce the compound's absorption and emission properties, we briefly discuss the ambient temperature optical spectra of FIrpic dissolved in CH_2Cl_2. (Figure 1) Assignments of the observed transitions, also depicted in Figure 1, are made in analogy to recent room temperature investigations of FIrpic dissolved in THF.[31] The classifications given can only be taken as rough description, since states assigned as LC always contain MLCT character

(12) Mathai, M. K.; Choong, V.-E.; Choulis, S. A.; Krummacher, B.; So, F. *Appl. Phys. Lett.* **2006**, *88*, 243512. (1−3).
(13) Shih, P.-I.; Chien, C.-H.; Chuang, C.-Y.; Shu, C.-F.; Yang, C.-H.; Chen, J.-H.; Chi, Y. *J. Mater. Chem.* **2007**, *17*, 1692–1698.
(14) Cai, X.; Padmaperuma, A. B.; Sapochak, L. S.; Vecchi, P. A.; Burrows, P. E. *Appl. Phys. Lett.* **2008**, *92*, 083308. (1−3).
(15) Shih, P.-I.; Chien, C.-H.; Wu, F.-I.; Shu, C.-F. *Adv. Funct. Mater.* **2007**, *17*, 3514–3520.
(16) Tanaka, D.; Agata, Y.; Takeda, T.; Watanabe, S.; Kido, J. *Jpn. J. Appl. Phys* **2007**, *46*, L117-L119.
(17) Su, S.-J.; Sasabe, H.; Takeda, T.; Kido, J. *Chem. Mater.* **2008**, *20*, 1691–1693.
(18) Mulder, C. L.; Celebi, K.; Milaninia, K. M.; Baldo, M. A. *Appl. Phys. Lett.* **2007**, *90*, 211109. (1−3).
(19) D'Andrade, B. W.; Thompson, M. E.; Forrest, S. R. *Adv. Mater.* **2002**, *14*, 147–151.
(20) Yu, X.-M.; Kwok, H.-S.; Wong, W.-Y.; Zhou, G.-J. *Chem. Mater.* **2006**, *18*, 5097–5103.
(21) Adamovich, V. I.; Cordero, S. R.; Djurovich, P. I.; Tamayo, A.; Thompson, M. E.; D'Andrade, B. W.; Forrest, S. R. *Org. Electron.* **2003**, *4*, 77–87.
(22) Su, Z.; Li, W.; Che, G.; Xu, M.; Kong, Z.; Wang, D.; Xin, Q.; Han, L.; Chu, B.; Bi, D. *Appl. Phys. Lett.* **2007**, *90*, 143505. (1−3).
(23) Orselli, E.; Kottas, G. S.; Konradsson, A. E.; Coppo, P.; Fröhlich, R.; De Cola, L.; van Dijken, A.; Büchel, M.; Börner, H. *Inorg. Chem.* **2007**, *46*, 11082–11093.
(24) Muegge, B. D.; Richter, M. M. *Anal. Chem.* **2004**, *76*, 73–77.
(25) Tanaka, I.; Tabata, Y.; Tokito, S. *Chem. Phys. Lett.* **2004**, *400*, 86–89.
(26) Tanaka, I.; Tokito, S. In *Highly Efficient OLEDs with Phosphorescent Materials*; Yersin, H., Ed.; Wiley-VCH: Weinheim, 2008; pp 283−309.
(27) Lee, C.-L.; Yang, X.; Greenham, N. C. *Phys. Rev. B* **2007**, *76*, 245201. (1−5).
(28) Huang, S.-P.; Jen, T.-H.; Chen, Y.-C.; Hsiao, A.-E.; Yin, S.-H.; Chen, H.-Y.; Chen, S.-A. *J. Am. Chem. Soc.* **2008**, *130*, 4699–4707.
(29) Thompson, J.; Arima, V.; Matino, F.; Berkebile, S.; Koller, G.; Netzer, F. P.; Ramsey, M. G.; Cingolani, R.; Blyth, R. I. R. *Synth. Met.* **2005**, *153*, 233–236.
(30) Kodate, S.; Suzuka, I. *Jpn. J. Appl. Phys.* **2006**, *45*, 574–578.
(31) Rausch, A. F.; Homeier, H. H. H.; Djurovich, P. I.; Thompson, M. E.; Yersin, H. *Proc. SPIE* **2007**, *6655*, 66550F. (1−16).
(32) Lamansky, S.; Thompson, M. E.; Adamovich, V.; Djurovich, P. I.; Adachi, C.; Baldo, M. A.; Forrest, S. R.; Kwong, R. U. S. Patent 20050214576, 2005.

and vice versa (compare also ref 33). Moreover, the states do not represent pure singlets or pure triplets, as SOC can mix states with different multiplicity.[31,33,34]

In the energy region above $\approx$ 29400 cm^{-1} (340 nm) the absorption spectrum shows a broad and intense band with a maximum at 39200 cm^{-1} (255 nm). In this range, one finds ligand-centered (LC) transitions involving the (4,6-dFppy) ligands and presumably also the (pic) ligand. In contrast to the high energy bands, the lower lying absorptions down to $\approx$ 21300 cm^{-1} (470 nm) cannot be found in the absorption spectrum of the free ligand. This indicates that the states exhibit strong MLCT (Ir5d-(4,6-dFppy)π^*) character. The intense transitions correspond to ^{1}MLCT states, while the weak low energy absorptions below $\approx$ 22700 cm^{-1} (440 nm) represent largely spin-forbidden transitions from the singlet ground state S_0 to the lowest triplet states. The peak at 21900 cm^{-1} (457 nm) (scaled by a factor of 20) overlaps with the high energy emission flank and is assigned to correspond to the electronic 0−0 transition between the singlet ground state and the lowest triplet state T_1. Because the $S_0 \rightarrow T_1$ transition is clearly observable, a significant ^{1}MLCT admixture to the emitting triplet state is indicated.

The 300 K emission spectrum of FIrpic in CH_2Cl_2 exhibits a maximum at 21300 cm^{-1} (469 nm), which is related to the electronic 0−0 transition from the lowest triplet state to the ground state. The transition at lower energy at 20200 cm^{-1} (496 nm) is assigned to stem from overlapping vibrational satellites. This will be substantiated in section 3.3.3. The spectrum is significantly less resolved than the one of $Ir(btp)_2(acac)$ (btp^- = (2-benzothienyl)-pyridinate, $acac^-$ = acetylacetonate),[35] for example, but it is much better resolved than the emission spectrum of $Ir(ppy)_3$ (ppy^- = 2-phenylpyridinate) under comparable conditions.[36] This behavior indicates different degrees of MLCT character in the emitting T_1 state of these compounds. A large MLCT character in the T_1 state is usually connected to larger inhomogeneity effects and to pronounced metal−ligand vibrational satellites in an energy region below 600 cm^{-1} relative to the electronic origin. Thus, these low-energy vibrational satellites lead to a smearing out of the spectra at ambient temperature.[37,38] Therefore, the shape of the room temperature spectrum indicates already a significant MLCT character of the emitting triplet state. This interpretation is also supported by the short emission decay time of 1.9 μs in degassed CH_2Cl_2 in combination with the high photoluminescence quantum yield. (For further arguments see below in section 4.)

With THF as solvent at T = 300 K, the absorption spectrum of FIrpic is only slightly modified, while the emission maximum is red-shifted by 180 cm^{-1} ($\approx$ 4 nm). The emission decay time in degassed THF amounts to 1.8 μs.

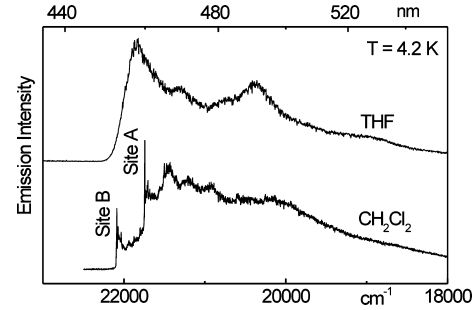

Figure 2. Emission spectra of $Ir(4,6\text{-}dFppy)_2(pic)$ (FIrpic) in the polycrystalline hosts THF ($c \approx 1 \times 10^{-5}$ mol/L) and CH_2Cl_2 ($c \approx 5 \times 10^{-5}$ mol/L), respectively, at T = 4.2 K after excitation at 355 nm. In THF, highly resolved spectra could not be obtained, whereas in a CH_2Cl_2 matrix two discrete sites, labeled site A and B, are observed together with a relatively intense inhomogeneous background.

3.2. Selection of a Suitable Host for High-Resolution Spectroscopy. The investigations at ambient temperature, presented in section 3.1, allow only a crude characterization of the emitting triplet state of FIrpic. More detailed information can be gained by carrying out emission and excitation measurements at low-temperature in a suitable matrix. For materials with largely planar structures, like many organic molecules[39−41] and organometallic Pd(II)[42,43] or Pt(II)[44−46] compounds, polycrystalline *n*-alkanes have proven to be suitable hosts for matrix isolation spectroscopy at liquid helium temperatures (Shpol'skii spectroscopy[39]). In the case of quasi-octahedral Ir(III) compounds, only a few examples are known, for which highly resolved spectra have been obtained in polycrystalline matrixes.[35,47−49] Recently, it has been shown that CH_2Cl_2 cooled to cryogenic temperatures represents a suitable host material for several Ir(III) compounds. For example, the red emitting $Ir(btp)_2(acac)$ could be characterized in detail when doped into this matrix.[35,48,50] Figure 2 shows emission spectra of FIrpic at T = 4.2 K measured in CH_2Cl_2 and in THF, respectively. The spectrum in THF is not much better resolved than at T = 77 K.[31] It is only slightly more structured than the ambient temperature spectrum, and no sharp lines can be observed. The high

(33) Nozaki, K. *J. Chin. Chem. Soc.* **2006**, *53*, 101–112.
(34) Miki, H.; Shimada, M.; Azumi, T.; Brozik, J. A.; Crosby, G. A. *J. Phys. Chem.* **1993**, *97*, 11175–11179.
(35) Finkenzeller, W. J.; Hofbeck, T.; Thompson, M. E.; Yersin, H. *Inorg. Chem.* **2007**, *46*, 5076–5083.
(36) Finkenzeller, W. J.; Yersin, H. *Chem. Phys. Lett.* **2003**, *377*, 299–305.
(37) Yersin, H.; Huber, P.; Wiedenhofer, H. *Coord. Chem. Rev.* **1994**, *132*, 35–42.
(38) Colombo, M. G.; Brunold, T. C.; Riedener, T.; Güdel, H.; Förtsch, M.; Bürgi, H.-B. *Inorg. Chem.* **1994**, *33*, 545–550.
(39) Shpol'skii, E. V. *Sov. Phys. Usp. (Engl. Transl.)* **1960**, *3*, 372–389.
(40) Murao, T.; Azumi, T. *J. Chem. Phys.* **1979**, *70*, 4460–4467.
(41) Jansen, G.; Noort, M.; van Dijk, N.; van der Waals, J. H. *Mol. Phys.* **1980**, *39*, 865–880.
(42) Yersin, H.; Schützenmeier, S.; Wiedenhofer, H.; von Zelewsky, A. *J. Phys. Chem.* **1993**, *97*, 13496–13499.
(43) Yersin, H.; Donges, D.; Nagle, J. K.; Sitters, R.; Glasbeek, M. *Inorg. Chem.* **2000**, *39*, 770–777.
(44) Yersin, H.; Donges, D. *Top. Curr. Chem.* **2001**, *214*, 81–186.
(45) Yersin, H.; Donges, D.; Humbs, W.; Strasser, J.; Sitters, R.; Glasbeek, M. *Inorg. Chem.* **2002**, *41*, 4915–4922.
(46) Donges, D.; Nagle, J. K.; Yersin, H. *Inorg. Chem.* **1997**, *36*, 3040–3048.
(47) Marchetti, A. P.; Deaton, J. C.; Young, R. H. *J. Phys. Chem. A* **2006**, *110*, 9828–9838.
(48) Finkenzeller, W. J.; Thompson, M. E.; Yersin, H. *Chem. Phys. Lett.* **2007**, *444*, 273–279.
(49) Wang, X.; Li, J.; Thompson, M. E.; Zink, J. I. *J. Phys. Chem. A* **2007**, *111*, 3256–3262.
(50) Yersin, H.; Finkenzeller, W. J. In *Highly Efficient OLEDs with Phosphorescent Materials*; Yersin, H., Ed.; Wiley-VCH: Weinheim, 2008; pp 1−97.

energy and the low energy peak correspond to the region of the inhomogeneously broadened electronic and overlapping vibrational satellite transitions, respectively. These peaks exhibit half-widths of about 500 cm^{-1}. However, we cannot exclude that, apart from the inhomogeneous broadening, also homogeneous broadening due to electron−phonon coupling might play a role.[50]

On the other hand, applying the CH_2Cl_2 matrix, two narrow lines with half-widths of 3 cm^{-1} are observed. They are accompanied by an intense broadband emission. As will be shown below, the lines represent electronic 0−0 transitions corresponding to two different sites of FIrpic in the polycrystalline CH_2Cl_2 host. Site A exhibits its dominant emission line at 21738 cm^{-1} and site B at 22080 cm^{-1}. Also in this host material, the relatively strong background is assigned to be induced mainly by an inhomogeneous distribution of the dopants.

By analogy to the extensive investigations carried out in the scope of the Shpol'skii spectroscopy,[39−46] we assign a specific site to a dopant that substitutes a defined small number of host molecules in the host crystallite and that experiences a defined environment. A different site is characterized, for example, by a different number of replaced host molecules. Very often, the number of different sites and their respective intensities depend on the conditions of crystallization, such as cooling rate,[51] tempering,[51] and doping concentration.[52]

3.3. Site-Selective Spectroscopy of Ir(4,6-dFppy)$_2$(pic) (FIrpic) in a CH_2Cl_2 Matrix. A deeper insight into the properties of an individual site of FIrpic doped in CH_2Cl_2 is gained at low temperatures by selectively exciting molecules of this site with a tunable dye laser and analyzing the respective electronic, vibronic, and decay properties.

3.3.1. Electronic Origins and Energy Level Diagrams. In Figure 3, site-selectively excited emission spectra and a site-selectively detected excitation spectrum are displayed for the region of the electronic origins of site A. The fact that the dopant molecules corresponding to site A and site B can be excited selectively and that their emission can be detected selectively proves the occurrence of different and individual sites.

The emission spectrum measured at $T = 1.8$ K shows one intense line at 21738 cm^{-1}. This line represents the purely electronic 0−0 transition I(A) → 0(A). It is accompanied by a weak phonon satellite which occurs 13 cm^{-1} lower in energy. A satellite of this energy is found for all purely electronic transitions for both sites A and B. It is assigned to a local vibrational mode of FIrpic in its matrix cage (local phonon mode). With increasing temperature an additional line appears at 21747 cm^{-1}, lying 9 cm^{-1} higher in energy than the dominant peak at 21738 cm^{-1}. This line results from the electronic 0−0 transition II(A) → 0(A). With further temperature increase, line II(A) gains intensity, but even at $T = 15$ K line I(A) is still the most intense one. When an excitation energy corresponding to a vibrational satellite of the 0(A) → III(A) transition is chosen, the electronic 0−0 transition III(A) → 0(A) can be detected at temperatures above ≈ 15 K (not shown). As expected, this emission line lies at 21814 cm^{-1}, that is, at the same energy as in the excitation spectrum (Figure 3a). However, because of thermal broadening effects like electron−phonon coupling, the spectrum is increasingly smeared out at temperatures above 15 K.

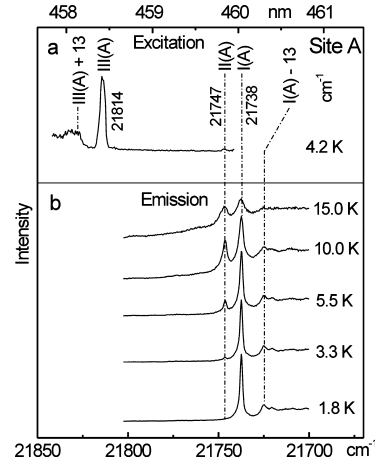

Figure 3. Site-selective spectra of the region of the electronic origins of site A of Ir(4,6-dFppy)$_2$(pic) (FIrpic) in CH_2Cl_2 ($c \approx 5 \times 10^{-5}$ mol/L). (a) Site-selectively detected excitation spectrum recorded at $T = 4.2$ K. The emission is detected at an energy of 21738 cm^{-1}, which corresponds to the purely electronic transition I(A) → 0(A). (b) Emission spectra recorded after selective excitation of substate III(A) at 21814 cm^{-1}.

The emission line I(A) → 0(A) at 21738 cm^{-1} was chosen as detection energy for the excitation spectrum (Figure 3a). This spectrum shows two excitation peaks at 21747 cm^{-1} (0(A) → II(A)) and 21814 cm^{-1} (0(A) → III(A)). They are in resonance with the corresponding emission lines as expected for electronic 0−0 transitions. Again, line 0(A) → III(A) is accompanied by a 13 cm^{-1} local phonon satellite. The excitation spectrum reveals further that the transition 0(A) → III(A) is by a factor of 60 more allowed than the transition 0(A) → II(A). Thus, the transition between triplet substate III(A) and the singlet ground state 0(A) carries by far the highest oscillator strength (radiative allowedness) and mainly governs the emission of this site even at ambient temperature. This is supported by an analysis of the individual triplet substate decay times, which will be presented in section 3.3.2.

As already pointed out, the emission spectrum of FIrpic in polycrystalline CH_2Cl_2 reveals a second prominent site (site B), which is blue-shifted by 342 cm^{-1} compared to site A. A similar energy separation between different sites has, for example, been found for Ir(btp)$_2$(acac).[35] The T_1 term of site B and its substates can be identified similarly as described above for site A. Figure 4 summarizes the energy level diagrams for the T_1 states of both sites of FIrpic in polycrystalline CH_2Cl_2. The individual decay times of the substates, as discussed in section 3.3.2, are also given.

The amount of ZFS is correlated to the efficiency of SOC and to the MLCT character of the emitting state.[5,31,33,44,50] Thus, it can be concluded that the emitting states of FIrpic

(51) Wiedenhofer, H. Ph. D. Thesis, Universität Regensburg, 1994.
(52) Meyer, B. *Low Temperature Spectroscopy*; American Elsevier Publ. Co.: New York, 1971.

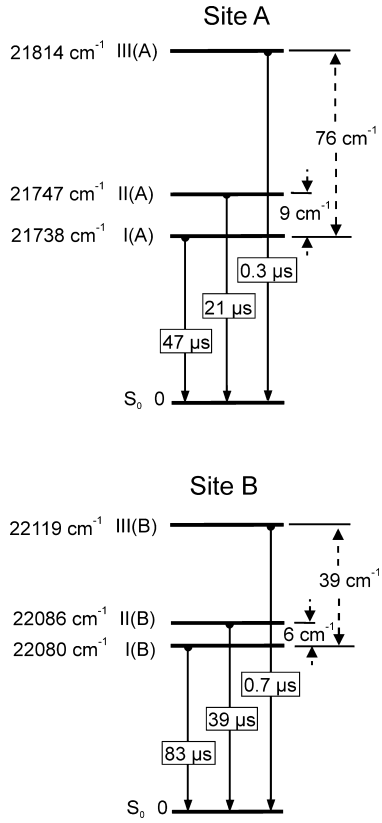

Figure 4. Energy level diagrams and decay times of the T_1 substates of Ir(4,6-dFppy)$_2$(pic) (FIrpic) in CH_2Cl_2 for the sites A and B. The emitting states of the two sites exhibit distinctly different ZFSs and decay times.

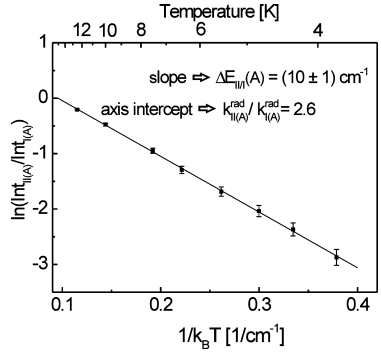

Figure 5. Boltzmann plot of the emission intensity ratio for the electronic 0−0 transitions II(A) → 0(A) and I(A) → 0(A) versus $1/k_BT$ for site A. The slope of the fit gives the energy separation between the substates I(A) and II(A), while the axis intercept displays the ratio of the radiative rate constants of the electronic 0−0 transitions.

in the sites A and B in a CH_2Cl_2 host exhibit distinctly different MLCT contributions. These properties will be further addressed below.

Figure 5 shows a Boltzmann plot of the emission intensity ratio of the purely electronic transitions II → 0 and I → 0 versus $1/k_BT$ for the T_1 state of site A together with a fit of the experimental data according to the equation

$$\ln\left(\frac{\mathrm{Int}_{\mathrm{II(A)}}}{\mathrm{Int}_{\mathrm{I(A)}}}\right) = \ln\left(\frac{k^{\mathrm{rad}}_{\mathrm{II(A)}}}{k^{\mathrm{rad}}_{\mathrm{I(A)}}}\right) - \frac{\Delta E_{\mathrm{II/I}}(\mathrm{A})}{k_{\mathrm{B}}T} \qquad (1)$$

wherein $\mathrm{Int}_{\mathrm{I(A)}}$ and $\mathrm{Int}_{\mathrm{II(A)}}$ represent the intensities of the 0−0 transitions I(A) → 0(A) and II(A) → 0(A). $k^{\mathrm{rad}}_{\mathrm{I(A)}}$ and $k^{\mathrm{rad}}_{\mathrm{II(A)}}$ are the corresponding radiative rate constants. $\Delta E_{\mathrm{II/I}}(\mathrm{A})$ represents the energy separation between the substates I(A) and II(A), k_B is the Boltzmann constant. Equation 1 holds only if the states involved are in a fast thermal equilibrium.[53−57] From the good fit of the experimental data, it can be conluded that the T_1 substates I and II are thermally equilibrated in the depicted temperature range and that processes of spin−lattice relaxation (SLR) between the two substates are fast.[56,57]

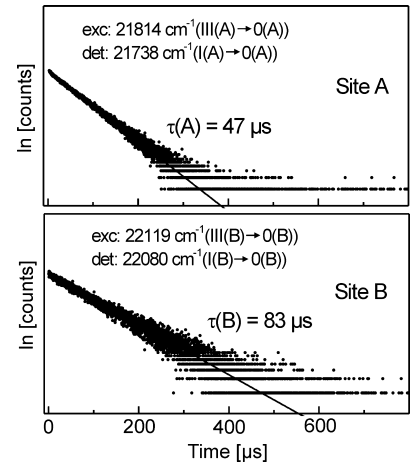

Figure 6. Emission decay curves of site A and site B of Ir(4,6-dFppy)$_2$(pic) (FIrpic) in CH_2Cl_2 measured at $T = 1.7$ K. The emission was detected at the energy of the respective transition I → 0 after pulsed excitation into the corresponding T_1 substate III.

From the slope of the plot in Figure 5 an energy separation between the substates I(A) and II(A) of (10 ± 1) cm^{-1} is obtained. The good accordance of the energy separation $\Delta E_{\mathrm{II/I}}(\mathrm{A})$ resulting from this Boltzmann fit to the value determined from the highly resolved spectra (Figure 3) shows that the involved substates belong to the same parent T_1 term, since the involvement of a state of a different site and a fast equilibration between these states because of fast energy transfer are very unlikely. The ordinate axis intercept provides the ratio $k^{\mathrm{rad}}_{\mathrm{II(A)}}/k^{\mathrm{rad}}_{\mathrm{I(A)}}$, which reveals that the purely electronic 0−0 transition II(A) → 0(A) is by a factor of 2.6 more allowed than the I(A) → 0(A) transition.

3.3.2. Decay Dynamics. The results described in section 3.3.1 reveal that the lowest triplet states of the sites A and B exhibit distinctly different ZFSs because of different MLCT perturbations and SOCs of the emitting T_1 substates to higher lying singlets and triplets. (Compare section 4.) Consequently, it is expected that the decay times of the triplet substates also vary for the different sites. At low temperature, for example, below 2 K, the emissions from the higher lying substates II and III are frozen out, and thus, the decay time of substate I can be measured directly. Figure 6 shows the corresponding emission decay curves of the T_1 state of site A and B at a temperature of 1.7 K. Both curves are

(53) Harrigan, R. W.; Crosby, G. A. *J. Chem. Phys.* **1973**, *59*, 3468–3476.
(54) Azumi, T.; O'Donnell, C. M.; McGlynn, S. P. *J. Chem. Phys.* **1966**, *45*, 2735–2742.
(55) Strasser, J.; Homeier, H. H. H.; Yersin, H. *Chem. Phys.* **2000**, *255*, 301–316.
(56) Yersin, H.; Strasser, J. *Coord. Chem. Rev.* **2000**, *208*, 331–364.
(57) Homeier, H. H. H.; Strasser, J.; Yersin, H. *Chem. Phys. Lett.* **2000**, *316*, 280–284.

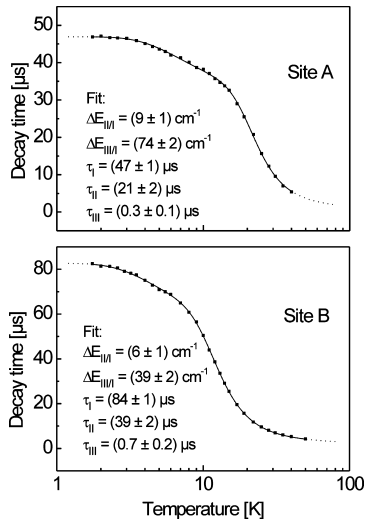

Figure 7. Emission decay time versus temperature for site A and B of Ir(4,6-dFppy)$_2$(pic) (FIrpic) doped into CH_2Cl_2. After selective excitation at the respective electronic 0−0 transition III → 0, the emission was detected at the 0−0 transition I → 0 of site A and B, respectively. A fit of eq 2 to the experimental data provides the energy separations $\Delta E_{II/I}$ and $\Delta E_{III/I}$ and the decay times of the individual triplet substates for each site.

monoexponential with time constants of $\tau_I(A) = 47\ \mu s$ and $\tau_I(B) = 83\ \mu s$.

The decay times of the higher lying T_1 substates II and III cannot be determined directly, since the measured emission decay at higher temperatures represents a thermalized emission of all three populated substates. However, an indirect method can be applied to determine the sublevel decay times, making use of the temperature dependence of the thermalized emission decay. For a system of three thermally equilibrated excited states, the rate constant for the depopulation k_{therm}, representing the inverse of the measured decay time τ_{therm}, is given by the expression[36,53−55]

$$k_{therm} = \frac{1}{\tau_{therm}} = \frac{k_I + k_{II}\exp\left(\frac{-\Delta E_{II}}{k_B T}\right) + k_{III}\exp\left(\frac{-\Delta E_{III}}{k_B T}\right)}{1 + \exp\left(\frac{-\Delta E_{II}}{k_B T}\right) + \exp\left(\frac{-\Delta E_{III}}{k_B T}\right)} \quad (2)$$

wherein k_I, k_{II}, and k_{III} are the rate constants for the depopulation of the individual triplet substates. $\Delta E_{II/I}$ and $\Delta E_{III/I}$ represent the energy separations between the substates.

In Figure 7, the emission decay times of site A and site B are plotted versus temperature. With increasing temperature, the decay becomes shorter for both sites, but a distinctly different temperature dependence is observed. For both sites, a plateau is present at low temperatures. For site A, it ends at about 4 K and for site B at about 2.5 K. These temperatures agree well with the growing in of the emission from the respective shorter living triplet substate II, as described in section 3.3.1.

A quantitative analysis of the decay time data according to a fit of eq 2 reveals the individual triplet substate properties of each site. As expected, the respective τ_I values determined by the fit match well to the measured emission decay times at $T = 1.7$ K, and the ZFS parameters are also in good agreement to those found from the high-resolution measurements (see section 3.3.1, Figure 4).

A comparison of the properties of the two sites shows that the decay times of all three T_1 sublevels are significantly shorter for site A than for site B. Again, this behavior is ascribed to a larger admixture of higher lying singlet states to the T_1 state of site A as compared to site B. This is consistent with the larger ZFS observed for site A. Remarkably, even the substates I of the two sites seem to be differently affected by singlet admixtures. However, it cannot be excluded that the decay times of substate I of the sites A and B are also differently influenced by nonradiative deactivation processes.

3.3.3. Vibrational Satellite Structures. In Figure 8, the selectively excited emission spectrum is reproduced for site A for $T = 1.5$ K. At this temperature, the emission stems only from substate I. The corresponding electronic 0−0 transition lies at 21738 cm^{-1} (compare section 3.3.1). The electronic origin is accompanied by emission lines of smaller intensity, which correspond to vibrational modes of the electronic ground state. Most vibrations in the energy range up to ≈100 cm^{-1} relative to the electronic origin represent vibrations of the dopant in its matrix cage.[58] Modes with energies up to ≈600 cm^{-1} represent mainly fundamentals with significant metal−ligand (M−L) character, but also low-energy intra-ligand vibrations can occur in this range.[44] The occurrence of M−L vibrational satellites with remarkable intensity is an indication of significant MLCT character in the T_1 state.[37,38,44] High energy fundamentals above ≈600 cm^{-1} largely correspond to internal vibrational modes of the ligands.[44,50]

In Table 1, all clearly observable intra-ligand (I-L) vibrational satellites of Ir(4,6-dFppy)$_2$(pic) (determined from the spectrum shown in Figure 8) are compared to corresponding modes found for Ir(4,6-dFppy)$_2$(acac) and for Pt(4,6-dFppy)(acac) (both taken from ref 59). Further, these energies are compared to those of the free (4,6-dFppy) ligand. Most modes can be well correlated. This indicates that the intra-ligand vibrational satellites found in the emission spectrum of substate I of Ir(4,6-dFppy)$_2$(pic) involve the (4,6-dFppy) ligand, while the ancillary ligand (pic) is very probably not active in the emission process. Accordingly, the $T_1 \leftrightarrow S_0$ transition is largely confined to the metal and the (4,6-dFppy) ligand. This assignment is supported by recent spectroscopic and theoretical investigations of FIrpic reported by You and co-workers.[60]

Because the electronic 0−0 transition I → 0 represents by far the most intense peak in the 1.5 K emission spectrum of site A (Figure 8), it can be concluded that the electronic transition is allowed by direct SOC, in contrast, for example, to spin-vibronic coupling.[44,61] This strongly indicates that

(58) Becker, D.; Yersin, H.; von Zelewsky, A. *Chem. Phys. Lett.* **1995**, *235*, 490–496.
(59) Rausch, A. F.; Homeier, H. H. H.; Yersin, H. In *Topics in Organometallic Chemistry - Photophysics of Organometallics*; Lees A. J., Ed.; Springer: Berlin/Heidelberg, 2009.
(60) You, Y.; Kim, K. S.; Ahn, T. K.; Kim, D.; Park, S. Y. *J. Phys. Chem. C* **2007**, *111*, 4052–4060.
(61) Albrecht, A. C. *J. Chem. Phys.* **1963**, *38*, 354–365.

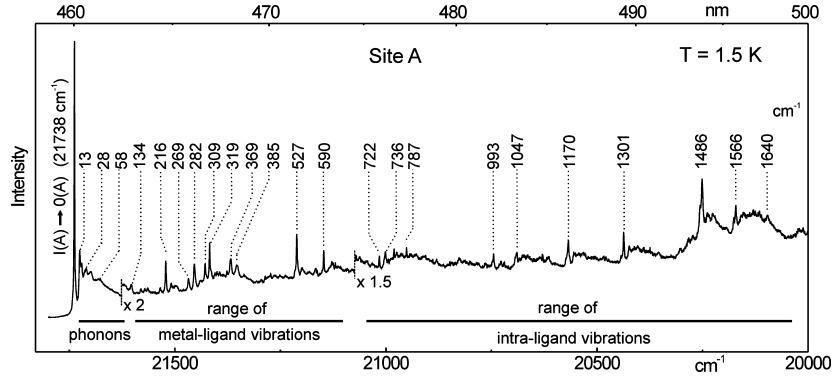

Figure 8. Emission spectrum of site A of Ir(4,6-dFppy)$_2$(pic) (FIrpic) in CH_2Cl_2 at $T = 1.5$ K. The sample was selectively excited at the 0−0 transition 0(A) → III(A) (21814 cm^{-1}). The values, which characterize the vibrational satellites, represent the energy differences in cm^{-1} relative to the electronic origin I(A) at 21738 cm^{-1}. Note the scaling factors given in the spectra.

Table 1. Comparison of Intra-Ligand Vibrational Energies As Determined from Emission Spectra of Site A of Ir(4,6-dFppy)$_2$(pic)[a], of Ir(4,6-dFppy)$_2$(acac),[b] and of Pt(4,6-dFppy)(acac)[c]. The compounds are dissolved in CH_2Cl_2. Vibrational energies of the free (4,6-dFppy) ligand, determined from a Raman spectrum ($T = 298$ K, neat ligand) are also given.

vibrational satellites in emission			Raman
Ir(4,6-dFppy)$_2$ (pic) [cm^{-1}]	Ir(4,6-dFppy)$_2$ (acac) [cm^{-1}]	Pt(4,6-dFppy) (acac) [cm^{-1}]	4,6-dFppy [cm^{-1}]
722	721		
736	737	739	740
787	788		785
993	996	994	994
1047	1046		
		1054	1056
1170	1170	1165	
1301	1301	1304	1305
1486	1487	1488	
1566	1564	1563	1570
1640	1640		

[a] $T = 1.5$ K, electronic 0-0 transition I → 0 at 21738 cm^{-1}. [b] Ref 59; $T = 1.5$ K, electronic 0-0 transition I → 0 at 21025 cm^{-1}. [c] Ref 59; $T = 4.2$ K, electronic 0-0 transition II/III → 0 at 21867 cm^{-1}.

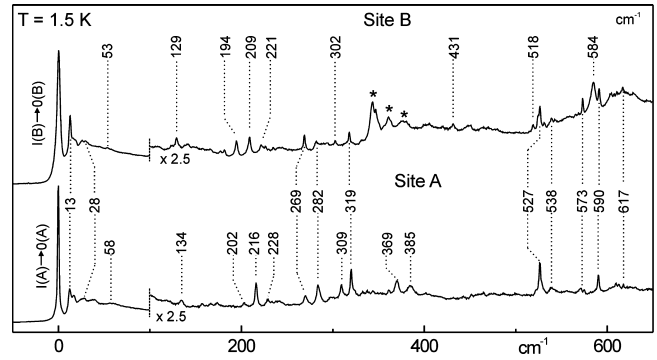

Figure 9. Comparison of emission spectra of site A and site B of Ir(4,6-dFppy)$_2$(pic) (FIrpic) in CH_2Cl_2 at $T = 1.5$ K in the energy region up to 650 cm^{-1} from the respective electronic 0−0 transition I → 0. The sample was selectively excited at the respective transition 0 → III. For a better comparison of the vibrational satellite structures, the spectra are shifted in energy so that their 0−0 transitions match. The values given at the vibrational satellites are the energy differences from the respective 0−0 transition. The spectrum of site B shows several lines which result from site A, these lines are marked with asterisks. Note the scaling factors given in the spectra.

the vibrational satellite structure largely stems from Franck−Condon (FC) activity.[44,61−65] For example, for the most intense vibrational satellites found in the emission of the substates II/III of Pt(4,6-dFppy)(acac) (Table 1), weak Franck−Condon progressions (e.g., 2 × 1054 cm^{-1}, 2 × 1488 cm^{-1}) have been observed.[59] However, in the emission spectrum of site A of FIrpic at $T = 1.5$ K progressions cannot be identified above the relatively strong background, presumably because of small Huang−Rhys parameters.[44,61−65] This behavior indicates that the geometries of the triplet substate I and of the electronic ground state 0 are very similar, at least in a rigid host cage. Presumably, this holds also for the two other triplet substates II and III.

In Figure 9, the emission spectra of the sites A and B at $T = 1.5$ K are reproduced for an energy range of 650 cm^{-1} relative to the respective electronic origin. In this range, one finds mainly local phonon and M−L vibrational satellites. For a better comparison, the spectra have been shifted by 342 cm^{-1}, that is, the respective electronic 0−0 transitions I → 0 are set to the same energy.

Interestingly, both spectra exhibit distinct differences of their vibrational satellite structures. Several modes are selectively active in the emission of FIrpic in site A or site B (e.g., A: 309 cm^{-1}, B: 194 cm^{-1}), while other satellites compare well in energy, but exhibit different intensities (e.g., the mode at 282 cm^{-1}). These differences may result from a relatively large sensitivity of the potential hypersurfaces on the respective host cage, which would particularly influence spin-vibronic coupling activity.[44,62−65] It is remarked that the satellite structure in the range of the intra-ligand modes above ≈ 600 cm^{-1} does not show the corresponding site dependence (not shown). This behavior supports a suggestion made in ref 44 that spin-vibronic activity in organo-transition metal complexes with heavy metal ions is frequently induced by M−L modes. In summary, the low-energy M−L satellites are more sensitive to the individual cage structure, that is, the environment of the dopant, than the high-energy intra-ligand satellites.

3.4. Investigation of FIrpic in THF. It is expected that a distinct dependence on the individual host environment, as observed for two discrete sites in CH_2Cl_2, occurs also in

(62) Ballhausen, C. J. *Molecular Electronic Structures of Transition Metal Complexes*; McGraw-Hill: New York, 1979.
(63) Henderson, B.; Imbusch, G. F. *Optical Spectroscopy of Inorganic Solids*; Clarendon: Oxford, 1989.
(64) Denning, R. G. In *Vibronic Processes in Inorganic Chemistry*; Flint, C. D., Ed.; Kluwer: Dordrecht, 1989.
(65) Fischer, G. *Vibronic Coupling*; Academic Press: London, 1984.

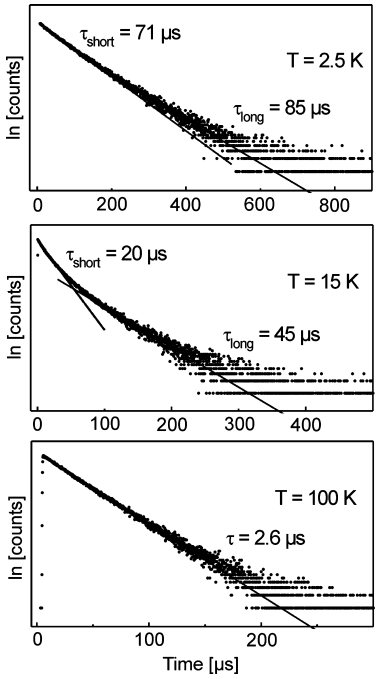

Figure 10. Emission decay curves of Ir(4,6-dFppy)$_2$(pic) (FIrpic) in THF ($c \approx 10^{-5}$ mol/L) at selected temperatures. The emission was detected at 21700 cm^{-1} after pulsed excitation at 355 nm. The decay curves at $T = 2.5$ K and $T = 15$ K are not monoexponential. For a simple approximation, short (τ_{short}) and long (τ_{long}) components as marked in the corresponding diagrams are used (see text).

other polycrystalline matrixes, such as in THF. As shown in section 3.2, for the THF host only broadband spectra are obtained even at $T = 4.2$ K. Thus, a direct determination of the individual triplet substate properties is not feasible. However, an indirect method, making use of the temperature dependence of the thermalized emission decay time as discussed above, provides the required information.

Figure 10 reproduces the emission decay curves of FIrpic doped into THF for temperatures of 2.5 K, 15 K, and 100 K. Obviously, the decay curves at $T = 2.5$ K and $T = 15$ K are not monoexponential, in contrast to the decay recorded at temperatures above 60 K. As an example, the decay at $T = 100$ K is shown. These properties do not depend on the concentration of the dopant in the range from $c \approx 10^{-4}$ to $\approx 10^{-6}$ mol/L. Thus, we conclude that energy transfer processes between adjacent emitter molecules are not responsible for the deviation from a monoexponential decay. Further, a correlation of the decay behavior with the detection energy is not seen.

In section 3.3, it is shown that discrete sites of FIrpic in CH_2Cl_2 exhibit clearly different ZFS parameters and emission decay times. For an extensive inhomogeneous distribution of dopants, as found in THF, it is expected that these parameters are spread over specific ranges. This assumption is supported by recent investigations of the ZFSs of the T_1 state of Ir(btp)$_2$(acac) in polymeric host matrixes by experiments of persistent spectral hole burning.[66] Thus, if the emission decay of an inhomogeneously broadened spectrum

(66) Bauer, R.; Finkenzeller, W. J.; Bogner, U.; Thompson, M. E.; Yersin, H. *Org. Electron.* **2008**, *9*, 641–648.

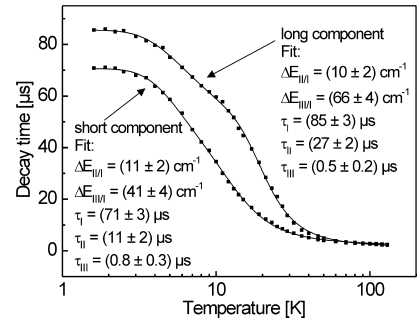

Figure 11. Emission decay time versus temperature of Ir(4,6-dFppy)$_2$(pic) (FIrpic) in THF ($c \approx 10^{-5}$ mol/L). The decay time data result from the short and long slope components, respectively, as estimated from the non-monoexponential decay curves. With these data, the fitting procedure according to eq 2 leads to the parameters given in the inset. These values represent a measure of the spread of the T_1 state properties in the inhomogeneous environment.

is monitored, contributions of many dopant ensembles, which are differently influenced by the host environment, are measured.

At low temperature, only substate I emits with different individual decay times of the various dopant ensembles. Therefore, the emission decay curve is non-monoexponential. Temperature increase leads to an increasing population of the higher lying T_1 substates II and III. The resulting population ratio, however, is different for the dissimilar ensembles with different energy separations $\Delta E_{II/I}$ and $\Delta E_{III/I}$. Thus, the larger the (inhomogenous) spreads of $\Delta E_{II/I}$ and $\Delta E_{III/I}$, the greater is the population difference of the respective substates II and III. As a consequence, the emission decay curves distinctly deviate from a monoexponential decay at intermediate temperatures. With further temperature increase, the thermalized emission decay times of the different ensembles deviate too little, and thus, the observed multiensemble decay largely appears to be monoexponential.

According to this model, the inhomogeneously distributed dopant molecules in a THF host do not all exhibit the same ZFS parameters and emission decay times of the substates. By simple approximations, a short- and long-time decay component can be extracted from each non-monoexponential decay curve in the temperature range 1.6 K $\leq T <$ 60 K. These data are plotted in Figure 11 together with the decay times obtained from the monoexponential curves in the temperature range $\approx$ 60 K $\leq T <$ 140 K. The fitting procedures, applying eq 2, provide two sets of fit data for the extreme ensembles of dopant molecules and thus give an approximate range for the triplet state data of FIrpic in the THF host. While the $\Delta E_{II/I}$ values do not vary significantly, the total ZFS covers a range from $\Delta E_{III/I}$ (short fit component) ≈ 41 cm^{-1} to $\Delta E_{III/I}$ (long fit component) ≈ 66 cm^{-1}. Also, the individual substate emission decay times vary clearly.

Interestingly, the two sites A and B of FIrpic doped into CH_2Cl_2 exhibit ZFS parameters and individual emission decay times of the T_1 substates which largely correspond to the extreme values as determined from the fit procedures for the THF host. (Compare Figure 4 and the fit data summarized in Figure 11.) This correspondence

shows that the model as discussed above is reasonable. In particular, the results clearly demonstrate that, also for the THF matrix, the T_1 state properties of FIrpic are strongly modified by the compound's environment.

4. Assignments and Conclusion

In the preceding sections, we have shown that important photophysical properties of the emitting triplet state of the OLED emitter Ir(4,6-dFppy)$_2$(pic) (FIrpic) are significantly affected by the environment of the dopants in polycrystalline matrixes. In particular, the ZFS of the emitting T_1 state, the decay times of the individual substates, and the vibrational satellite structures were found to depend on the individual site in the same matrix. For FIrpic doped into a CH_2Cl_2 host at cryogenic temperatures, two discrete sites are identified which exhibit ZFS values of 39 cm^{-1} and 76 cm^{-1}, respectively. On the other hand, the ZFS of the T_1 state of inhomogeneously distributed FIrpic molecules in frozen THF is spread over a range of 41 cm^{-1} < ΔE(ZFS) < 66 cm^{-1}. Also the emission decay times vary strongly.

According to an empirical ordering scheme, the magnitude of ZFS of the emitting T_1 state displays the effectiveness of SOC to higher lying states and can be correlated with the MLCT contribution in the emitting triplet.[5,44,50,67] It is remarked that the effectiveness of SOC strongly depends on the involvement of the central metal d-orbitals in the corresponding wave functions. Because of the mentioned correlation and the ΔE(ZFS) values found for FIrpic, the T_1 state can be assigned to be largely of MLCT character. A quantitative description of the triplet state properties based on quantum mechanical calculations is still very difficult. However, the effects of SOC on the ZFS of the T_1 term and on the radiative rates of the triplet substates can be illustrated by formulas based on second-order perturbation theory. The energy $E(i)$ of one specific triplet substate i of T_1 (with i = I, II, III) can be expressed by[31,50,68]

$$E(i) = E_{T_1} + \sum_{T_n} \frac{|\langle \phi_{T_n(j)} | \hat{H}_{SO} | \phi_{T_1(i)} \rangle|^2}{E_{T_1} - E_{T_n}} + \sum_{S_n} \frac{|\langle \phi_{S_n} | \hat{H}_{SO} | \phi_{T_1(i)} \rangle|^2}{E_{T_1} - E_{S_n}} \quad (3)$$

while the radiative rate constant $k^r(i)$ of T_1 substate i for the transition to the electronic ground state is given by[31,50,69]

$$k^r(i) = \text{const} \times \bar{\nu}^3 \times \left| \sum_{S_n} \frac{\langle \phi_{S_n} | \hat{H}_{SO} | \phi_{T_1(i)} \rangle}{E_{T_1} - E_{S_n}} \times \langle \phi_{S_0} | e\vec{r} | \phi_{S_n} \rangle \right|^2 \quad (4)$$

$\hat{H}_{SO}$ is the SOC Hamiltonian, and E_{T_1}, $E_{S_n}$and E_{T_n} are the unperturbed energies of the lowest triplet and of higher lying singlet and triplet states S_n and T_n, respectively. $T_n(j)$ characterizes a substate j of T_n. $\phi_{S_n}$and $\phi_{T_n(j)}$ represent the corresponding wave functions. In particular, they must have the same symmetry representation as the wave function $\phi_{T_1(i)}$ of T_1 substate i, otherwise, the matrix elements in eqs 3 and 4 vanish. $\bar{\nu}$ represents the transition energy to the ground state and $e\vec{r}$ is the electric dipole operator. The SOC matrix elements are usually different for the three T_1 substates. This leads to different energy stabilizations and thus, to the ZFS as well as to different radiative rates. Presumably, SOC with the next higher lying ^{3}MLCT state(s) dominates the individual energy stabilization of the T_1 substates and thus largely determines the ZFS because of the smaller energy denominators ($E_{T_1} - E_{T_n}$) as compared to ($E_{T_1} - E_{S_n}$), while the radiative rates stem only from SOC with higher lying singlet states.

Equations 3 and 4 demonstrate that SOC is crucial for the photophysical parameters being of interest here. However, SOC with higher lying singlet and triplet MLCT states is only effective, if T_1 is a ^{3}MLCT state or contains large ^{3}MLCT contributions, while the effects of SOC are small for an emitting triplet state of purely ligand centered character.[31,33,34,50,70,71] Further, efficient SOC requires that the considered MLCT states, that is, the states which mix according to eqs 3 and 4, involve *different* d-orbitals.[31,50] These considerations are important for the design of compounds with high radiative rates or short emission decay times. Short radiative decay times are crucial for emitters to be applied in OLEDs to induce high emission quantum yields and to reduce roll-off[72,73] and saturation effects.

For an explanation of the strong dependence of the ZFS and the individual T_1 sublevel decay times of FIrpic on the host environment, we have to take into account the well-known fact that MLCT states usually are more sensitive to environmental effects than LC states.[74−77] In particular, already slight changes of the local environment of the compound, which can, for example, be induced by steric effects, are expected to affect the energies and the splittings of the Ir(III) d-orbitals. As consequence, the energies of the MLCT states are altered. This results in modified energy denominators in eqs. 3 and 4 and thus, leads to changes of the ZFSs and of the individual radiative rates. Additionally, the matrix-induced shifts of the lowest ^{3}MLCT state relative to the lowest ^{3}LC state will result in variations of the extent of MLCT/LC mixing. Also, other matrix influences should not be neglected, but the discussion of these aspects is beyond the scope of this article (cf. ref 74).

The properties of triplet emitters can also be affected in amorphous matrixes as usually applied in OLEDs because of differences in the local environments. Corresponding investigations have not yet been carried out for FIrpic, but experiments of spectral hole burning at low temperatures have been performed with Ir(btp)$_2$(acac) doped in several

(67) Yersin, H.; Humbs, W.; Strasser, J. *Top. Curr. Chem.* **1997**, *191*, 153–249.
(68) Ikeda, S.; Yamamoto, S.; Nozaki, K.; Ikeyama, T.; Azumi, T.; Burt, J. A.; Crosby, G. A. *J. Phys. Chem.* **1991**, *95*, 8538–8541.
(69) Abedin-Siddique, Z.; Ohno, T.; Nozaki, K.; Tsubomura, T. *Inorg. Chem.* **2004**, *43*, 663–673.
(70) Azumi, T.; Miki, H. *Top. Curr. Chem.* **1997**, *191*, 1–40.
(71) Glasbeek, M. *Top. Curr. Chem.* **2001**, *213*, 95–142.
(72) Reineke, S.; Walzer, K.; Leo, K. *Phys. Rev. B* **2007**, *75*, 125328. (1−13).
(73) Giebink, N. C.; Forrest, S. R. *Phys. Rev. B* **2008**, *77*, 235215. (1−9).
(74) Chen, P.; Meyer, T. J. *Chem. Rev.* **1998**, *98*, 1439–1477.
(75) Ulstrup, J. *Charge Transfer Processes in Condensed Media, Lecture Notes in Chemistry*; Springer-Verlag: New York, 1979; Vol. *10*.
(76) Colombo, M. G.; Hauser, A.; Güdel, H. U. *Inorg. Chem.* **1993**, *32*, 3088–3092.
(77) Colombo, M. G.; Hauser, A.; Güdel, H. U. *Top. Curr. Chem.* **1994**, *171*, 143–171.

polymeric matrixes.[66] The obtained results agree with the experimental findings gained from studies in polycrystalline hosts[35,48,50] and support the model presented in this investigation.

In conclusion, we have demonstrated that polycrystalline host materials can have a distinct influence on photophysical properties of organo-transition metal compounds. Also for amorphous matrixes usually applied in OLEDs, a careful choice of the host material is definitely useful for optimizing emission properties. Thus, strategies for material development with regard to efficiency, emission decay time, and saturation and roll-off effects should take into account the emitter *and* its environment.

Acknowledgment. The *Bundesministerium für Bildung und Forschung (BMBF)* is gratefully acknowledged for providing the funding of this investigation. We thank the *BaCaTeC* for financial support of the exchange program of the University of Regensburg with the University of Southern California. We also thank Priv.-Doz. Dr. Alkwin Slenczka for measuring the Raman spectrum.

IC801250G